

Unsupervised Foreground-Background Segmentation with Equivariant Layered GANs

Yu Yang¹, Hakan Bilen², Qiran Zou¹, Wing Yin Cheung¹, Xiangyang Ji¹
¹Tsinghua University, BNRist ²The University of Edinburgh

yang-yu16@mails.tsinghua.edu.cn, hbilen@ed.ac.uk,
 {zouqr19, zhangyx20}@mails.tsinghua.edu.cn, xyji@tsinghua.edu.cn

Abstract

We propose an unsupervised foreground-background segmentation method via training a segmentation network on the synthetic pseudo segmentation dataset generated from GANs, which are trained from a collection of images without annotations to explicitly disentangle foreground and background. To efficiently generate foreground and background layers and overlay them to compose novel images, the construction of such GANs is fulfilled by our proposed Equivariant Layered GAN, whose improvement, compared to the precedented layered GAN, is embodied in the following two aspects. (1) The disentanglement of foreground and background is improved by extending the previous perturbation strategy and introducing private code recovery that reconstructs the private code of foreground from the composite image. (2) The latent space of the layered GANs is regularized by minimizing our proposed equivariance loss, resulting in interpretable latent codes and better disentanglement of foreground and background. Our methods are evaluated on unsupervised object segmentation datasets including Caltech-UCSD Birds and LSUN Car, achieving state-of-the-art performance.

1. Introduction

As deep neural networks continue to dramatically push the state-of-the-art in most supervised computer vision tasks, the interest of the community has shifted to developing methods that rely on minimal human supervision. Semantic segmentation that requires pixelwise labels is one of the computer vision tasks with most detailed and time consuming annotations. In this paper, we focus on a specific case of this problem, foreground-background segmentation – learning pixel-wise foreground and background segmentation from a collection of single-object images – *without any labels*.

Unsupervised foreground-background segmentation is

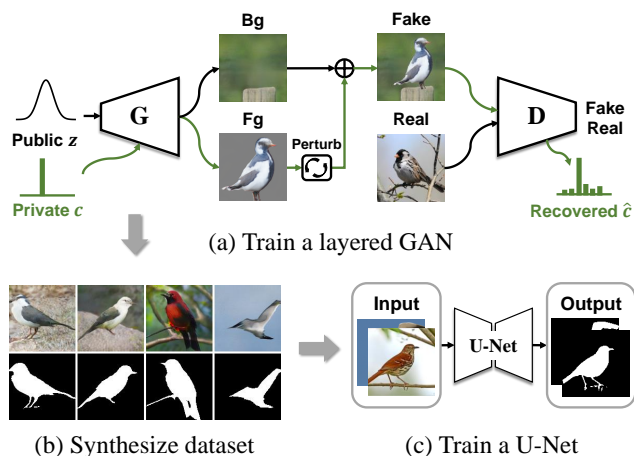


Figure 1: Unsupervised foreground-background segmentation. (a) Train a layered GAN which produces and overlays layers to generate images. (b) Synthesize images with pseudo-segmentation masks. (c) Train a segmentation network (U-Net) with the synthetic data.

a challenging task due to large intra-class variation in foreground, and small inter-class variation between foreground and background. Earlier work [47, 23, 28, 1, 6] on this topic, also known as co-segmentation, proposes to learn discriminating foreground and background pixels by use of shallow classifiers on hand-crafted features. More recently, the representations and per-pixel clustering have been learned simultaneously in deep neural networks [27, 41, 31]. To ensure that networks learn to group pixels with similar semantics, the per-pixel clustering is encouraged to be invariant to semantic-preserving transformations [27, 41]. Since these methods solve the problem in a patch-level, *i.e.* assigning labels to each (super-)pixel, they are limited in learning high-level semantic concepts like object entities. More recently, a promising line of work [7, 3, 58] is based on the Generative Adversarial Networks (GANs) [19], which can potentially learn the concept

of object categories and their whole extent due to its *generative* nature.

The state-of-the-art generative methods [7, 3] decompose visual scenes into foreground and background in *layered* generative models. ReDO [7] splits an image into regions with predicted masks and randomly replaces a region with the the generated one. PerturbGAN [3] learns layered representations (*i.e.* separate background and foreground), and overlays foreground on background to compose novel images. However, learning to generate images with decomposition does not guarantee that they are correctly factorized. In particular, trivial masks such as all-foreground, arbitrary, and all-background masks can emerge (see Fig. 2, Fig. 3 & Fig. 2 in [3]) without strongly regulating them. Motivated by these limitations, we propose an unsupervised foreground-background segmentation that builds on PerturbGAN [3] and we make the following three contributions to address them as following.

First, to mitigate the trivial solution of all-foreground, we build on PerturbGAN and substantially improve it by incorporating extensive geometric perturbations to the foreground layer. Originally PerturbGAN [3] blends the generated foreground and background pixels after applying a small random translation to the foreground ones, which result in unnatural boundary effects in the generated images when partially correct pixels or all pixels are associated with foreground. These unnatural effects are penalized by a discriminator. However, we observe that small translations alone are insufficient to learn disentangled representations that can independently model object pose and appearance and it cannot effectively address the trivial solutions. To this end, we propose to use a richer set of transformations including scaling, translation and rotation while training our generative model and show that this leads to a substantial gain in terms of image and segmentation quality.

Second, to prevent all-background mask, we introduce a new strategy, *private code recovery* that reconstructs private code of foreground from the composite image. As previously discussed perturbations cannot prevent generators from producing all-background mask, where any perturbation would not create artifacts, PerturbGAN [3] regulates this case by minimizing mask size loss $\mathcal{L}_{\text{size}} = \mathbb{E}_{\pi} \max\{0, \eta - |\pi|_1\}$, where $\pi \in [0, 1]^{H \times W}$ denotes mask and η is the minimal tolerable mask size. The hyperparameter η , however, is sensitive to object scale, category and dataset, making the mask size loss not a principled way. In contrast, we propose a principled method that incorporates a *private code* for generating foreground and is then recovered from the generated image and the private code. If all-background masks (*i.e.* zero masks) emerge, information of the private code would be erased and can not be transmitted to the generated images, making it impossible to recover the private code (see Fig. 3). Therefore, the private code recov-

ery could drive the generator to produce non-zero mask yet do not rely on hyperparameters and is more principled.

Third, to encourage better separation of foreground and background, we introduce a novel equivariance loss. An ideal segmentation method must disentangle foreground and background, which allows for more interpretable and disentangled latent representation. As an important property of neural network, equivariance [35] helps to learn interpretable and disentangled representation which is shown to benefit various computer vision tasks [60, 55, 39]. Therefore, following the definition of equivariance, we propose for the layer-wise generator an equivariance loss (Fig. 4 & Equ. (8)). We show that equivariance loss could help the layered GAN produce more precise masks, resulting in higher segmentation performance.

Our methods are evaluated with unsupervised object segmentation task on Caltech-UCSD Birds 200-2011, and LSUN Car. Experiment results show that our proposed modules could improve the ability of disentangling foreground and background for the layered GAN. The segmentation performance is also competitive compared to state-of-the-art methods.

2. Related Work

Unsupervised Object Segmentation. Earlier work [47, 23, 28, 1, 6] on unsupervised object segmentation utilise handcrafted features and model spatial smoothness. In the era of deep learning, the feature learning and per-pixel clustering are integrated with deep neural networks [27, 41, 31]. Constraints such as spatial smoothness [31] and transformation invariance [27, 41] are enforced to encourage pixels with similar semantics to be grouped. A recent concurrent work [49] propose to learn unsupervised segmentation by maximizing the inpainting error.

Another line of work adopts analysis by synthesis and integrates segmentation into deep generative models such as Variational Autoencoders (VAEs) [33] and Generative Adversarial Networks (GANs) [19]. VAE-based approaches [5, 20, 15, 37] have been successfully applied to complex synthetic scenes but seldom demonstrated on realistic scenes. GAN-based methods [7, 3, 58] could handle real-world scenes though currently limited to simple ones. In particular, ReDO [7] decomposes an image into regions with masks and replaces a random region with the generated one. Bielski & Favaro [3] propose perturbation strategy to spur the emergence of segmentation in their PerturbGAN. Voynov *et al.* [58] discover direction candidates in the latent space of pre-trained GAN (*e.g.* BigBiGAN [14]), manually identify the directions related to contrasting foreground-background, and obtain segmentation masks by processing reconstructed real images with latent directions. Our method is based on PerturbGAN [3]. Segmentation networks are trained on synthetic data generated

by GANs. This post-segmentation-training is also adopted by Voynov *et al.* [58], which is easier to be employed than training an image encoder as in [3].

Layered GANs. While standard GANs generate images in one pass, layered GANs generate images by generating and combining components, also known as image layers (*e.g.* background, foreground objects). This layer-wise generation is first introduced by AIR [16] in the context of VAE. Afterwards, Yang *et al.* propose LR-GAN [61], a GAN model that generates background image and recurrently generates foreground objects. GAN-based models could generate more realistic images than VAE-based models. Though successfully demonstrated on realistic datasets, however, LR-GAN is limited by the primitive GAN techniques. With the advance of GAN architectures and training techniques, layer-wise generation is observed to degenerate during training, resulting in all pixels labelled as one component. Some work [53, 2] address this issue by introducing separate component (*e.g.* background) discriminator, which leverages object bounding box annotations during training. Bielski & Favaro [3] prevent degeneration with perturbation strategy and a loss function that penalizes very small mask size, shaking off the requirement of any explicit manual labels like bounding boxes. Our layered GANs also apply perturbation and learn layer-wise generation without explicit manual labels. Different from [3], we rely on private code recovery to prevent degeneration rather than mask size penalty. Furthermore, a novel equivariance loss is introduced to promote learning layer-wise generation.

Equivariance. Equivariance, meaning representations vary in an correlated way of how images vary, is an important property of deep neural networks [35] and receives massive attention from the community. Equivariance can be imposed to the neural network by group-theoretic generalisation of convolutional layers [12, 11], Wavelets filters [4, 52, 42], capsule modules [48, 22], and specific loss functions [55, 24]. Equivariance is also shown beneficial for lots of practical computer vision problems such as representation learning [17, 63], classification [56], segmentation [10, 38, 24], landmark detection [55, 9] *etc.* . However, we notice that there is little work on the equivariance of *generators* in GANs. Jahanian *et al.* [26] propose to learn a trajectory in the latent space equivariant to a trajectory in the image space simultaneously with adversarial learning. Their method is shown beneficial for GAN steerability but limited to synthetic data and primitive GAN architectures. Dey *et al.* [13] substitute normal convolutional layers in the generator with the group-theoretically generalised convolutional layers for equivariance to translation and rotation. In contrast, our approach towards equivariance is learning-based which is demonstrated beneficial for layered

GANs and segmentation.

Interpretable Directions in GAN Latent Space. Earlier work [44, 29] discover that some directions in GAN latent space correspond to interpretable variation of features such as emotion, gender in face generation. More recent work analyse the latent space of trained GANs by exploiting human-provided supervision [18, 51, 29] or self-supervision [43, 26, 57], and mathematically analysing layer weights [54] or features [25], leading to discovery of substantial interpretable directions. Inspired by these work, we consider the linear walk regarding the transformation in latent space. However, our methods influence the training process of GANs, whereas these work only analyses the trained GANs.

3. Methods

Let $G : \mathcal{Z} \rightarrow \mathcal{X}$ be a generative model that maps a latent variable $\mathbf{z} \in \mathcal{Z}$ to an image $\mathbf{x} \in \mathcal{X}$. Regarding two-layer generation, G is decomposed into background generator G_b and foreground generator G_f as $G = (G_b, G_f)$. G_b generates background image \mathbf{x}_b and G_f generates foreground image \mathbf{x}_f with mask π . The whole generated image \mathbf{x} is obtained by blending \mathbf{x}_f and \mathbf{x}_b with π as alpha map,

$$\mathbf{x} = (1 - \pi) \odot \mathbf{x}_b + \pi \odot \mathbf{x}_f. \quad (1)$$

3.1. Spurring the Emergence of Semantic Layers

Standard GANs train G adversarially against discriminator D via optimising the following minimax problem

$$\min_G \max_D \mathbb{E}_{p_{\text{data}}(\mathbf{x})} f(D(\mathbf{x})) + \mathbb{E}_{\mathbf{z}} f(-D(G(\mathbf{z}))), \quad (2)$$

where $f : \mathbb{R} \rightarrow \mathbb{R}$ is a concave function whose form varies for different kinds of GANs.

In GANs, discriminator $D : \mathcal{X} \rightarrow \mathbb{R}$ is tasked to classify real and fake images. In a well-trained GAN, the generator could generate photo-realistic images which can hardly be discerned by discriminator. If layer-wise generation is adopted, however, there is no guarantee that semantic layers would emerge automatically. In particular, three kinds of trivial masks might emerge: i) *all-foreground-mask*, i.e. $\pi = \mathbf{1}$, ii) *arbitrary-mask*, iii) *all-background-mask*, i.e. $\pi = \mathbf{0}$. Correspondingly, the behaviour of layer generators is as follows. i) G_f generates the whole image while G_b could generate anything. ii) Both G_f and G_b generate the whole yet identical images. iii) G_b generates the whole image while G_f could generate anything. These trivial solutions are prevented by the following measures.

Layer perturbation. Bielski & Favaro [3] propose to perturb the position of foreground object before superimposition in the training process. Formally, it can be written as

$$\mathcal{T}_\epsilon^\mathcal{X} \mathbf{x} = (1 - \mathcal{T}_\epsilon^\mathcal{X}(\pi)) \odot \mathbf{x}_b + \mathcal{T}_\epsilon^\mathcal{X}(\pi) \odot \mathcal{T}_\epsilon^\mathcal{X}(\mathbf{x}_f), \quad (3)$$

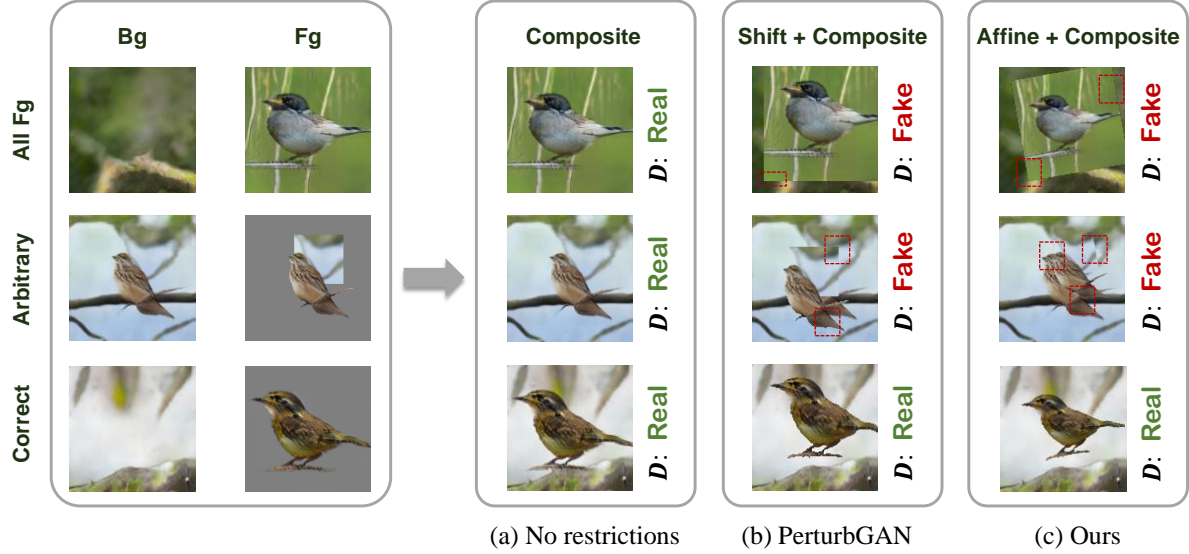


Figure 2: Layer perturbation. (a) Without any restriction, the discriminator can not penalise all-foreground mask and arbitrary masks. (b) PerturbGAN randomly shift the foreground. (c) We use a richer set of transformation, *i.e.* affine transformation, to make perturbation, which is more likely to cause artefacts.

where $\mathcal{T}_\epsilon^\mathcal{X}$ is abused as operating on the whole image and layers and is parameterized with ϵ . In PerturbGAN [3], $\mathcal{T}_\epsilon^\mathcal{X}$ is represented by pixel-unit translation. In this paper, $\mathcal{T}_\epsilon^\mathcal{X}$ is extended to differentiable affine transformation which is typically decomposed into three consecutive elementary transformation: isotropic scaling, rotation, and translation. Formally,

$$\mathcal{T}_\epsilon^\mathcal{X}(\mathbf{x})(u, v, 1) = \mathbf{x}(\mathbf{A}_\epsilon^{-1}(u, v, 1)), \quad (4)$$

$$\mathbf{A}_\epsilon = \mathbf{T}(t_x, t_y) \mathbf{R}(\alpha) \mathbf{S}(s), \text{ where } \mathbf{S}(s) = \begin{bmatrix} s & 0 & 0 \\ 0 & s & 0 \\ 0 & 0 & 1 \end{bmatrix}$$

$$\mathbf{T}(t_x, t_y) = \begin{bmatrix} 1 & 0 & t_x \\ 0 & 1 & t_y \\ 0 & 0 & 1 \end{bmatrix}, \mathbf{R}(\alpha) = \begin{bmatrix} \cos \alpha & -\sin \alpha & 0 \\ \sin \alpha & \cos \alpha & 0 \\ 0 & 0 & 1 \end{bmatrix}. \quad (5)$$

During training phase, parameters of $\mathcal{T}_\epsilon^\mathcal{X}$ are sampled from a specific uniform distribution, *e.g.* $\log_2 s \sim \mathcal{U}(-0.2, 0.2)$, $\alpha \sim \mathcal{U}(-15^\circ, 15^\circ)$, and $t_x, t_y \sim \mathcal{U}(-0.125, 0.125)$.

As explained in Fig. 2, if a layered GAN learns all-foreground mask or arbitrary mask, superimposing the perturbed foreground on the background pixels would cause artefacts (*e.g.* sharp and unnatural border) which would be discerned and penalised by the discriminator. Such artefacts are more likely to be triggered when richer perturbation, like affine transformation, is applied.

In contrast, if a layered GAN learns reasonable semantic layers, layer perturbation within small range would not hurt the realness of generated images. This is because fore-

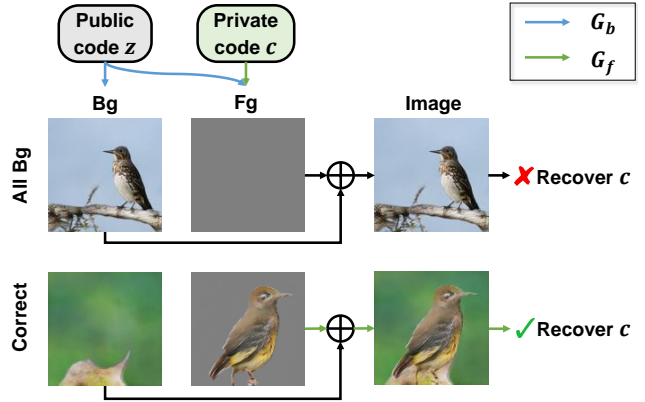


Figure 3: Private code recovery. Private code c is preserved only for generating foreground. All-background mask erase the information of c , making it impossible to recover c from generated images. Correct mask allows the information of c passing through composition, thus c could be recovered from generated images.

ground appears on the top among layers and the relative positions of foreground and background can typically be varied up to a certain degree.

Private code recovery. Despite the layer perturbation, the layered GAN is still probable to learn all-background mask. We introduce a novel principle, private code recovery, to mitigate this problem. Besides public code z which is shared across G_b and G_f , an additional private

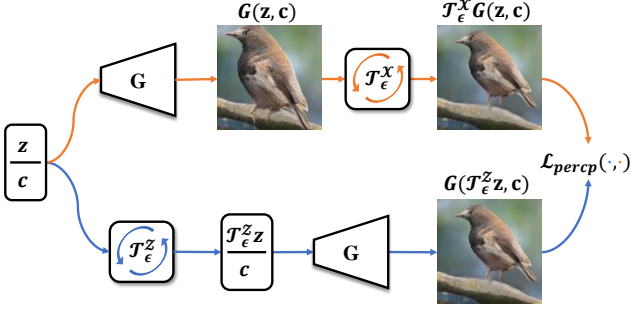


Figure 4: Equivariance loss. The equivariance loss drives the image generated from transformed latent codes, $G(\mathcal{T}_\epsilon^Z \mathbf{z}, \mathbf{c})$, to be close to the transformed generated images, $\mathcal{T}_\epsilon^X G(\mathbf{z}, \mathbf{c})$.

code \mathbf{c} is introduced and only reserved to G_f (Fig. 3). Typically, \mathbf{z} is continuous and assumed to observe normal distribution, *i.e.* $\mathbf{z} \sim \mathcal{N}(0, \mathbb{I})$, while \mathbf{c} is discrete and assumed to observe uniform categorical distribution. In this way, if all-background mask is learned, information of \mathbf{c} is erased by zero mask, making it impossible to reconstruct \mathbf{c} from \mathbf{x} . Otherwise, the information of \mathbf{c} could be transmitted through the superimposition with non-zero mask and \mathbf{c} could be recovered from \mathbf{x} .

Therefore, to encourage non-zero masks, an extra private code recovery task is introduced. Its loss can be written as

$$\mathcal{L}_r^{(G,E)} = \mathbb{E}_{\mathbf{z}, \mathbf{c}} \log E(\mathbf{c} | G(\mathbf{z}, \mathbf{c})), \quad (6)$$

where $E(\cdot | G(\mathbf{z}, \mathbf{c}))$ represents the posterior probability of \mathbf{c} given the generated image $\mathbf{x} = G(\mathbf{z}, \mathbf{c})$ estimated by E . Theoretically related to InfoGAN [8], Equ. (6) would maximize the mutual information $I(\mathbf{c}; G(\mathbf{z}, \mathbf{c}))$ between the private code and the generated image. Following the common practice [8, 36], E shares network layers except the last few ones with discriminator D and is jointly optimised with G via amortised variational inference. We refer to [8] and supplementary material for more details.

In contrast to PerturbGAN [3] that penalizes the output when mask size $|\pi|$ is lower than a prefixed threshold, our private code recovery is more principled and does not require to set an additional hyperparameter (e.g. minimum mask size η).

3.2. Towards Equivariant Latent Space

We propose to improve representation learning of the described layered GANs from equivariance perspective. Generally, if transformation of images can be encoded by certain transformation of representation, we call the representation, or the model that yield such representation, is equivariant to the transformation [35]. Formally, in our layered GANs, we say G is equivariant to a set of transformation \mathcal{E}

if

$$\mathcal{T}_\epsilon^X G(\mathbf{z}, \mathbf{c}) = G(\mathcal{T}_\epsilon^Z \mathbf{z}, \mathbf{c}), \quad (7)$$

where \mathcal{T}_ϵ^X and \mathcal{T}_ϵ^Z denote the transformations in image space \mathcal{X} and latent space \mathcal{Z} respectively, both indexed by $\epsilon \in \mathcal{E}$.

We consider \mathcal{T}_ϵ^X as affine transformation, *i.e.* Equ. (4) and define the index $\epsilon = (t_x, t_y, \alpha, \log_2 s)$. However, we are unaware of the representation of \mathcal{T}_ϵ^Z . Inspired by recent work on interpretable directions in GAN latent space [51, 26, 25, 57], we adopt the linear walk as the representation of \mathcal{T}_ϵ^Z and model it with neural network Φ as $\mathcal{T}_\epsilon^Z \mathbf{z} = \mathbf{z} + \Phi(\epsilon)$, where Φ is implemented with Multiple Layer Perceptron (MLP) and jointly trained with G .

To this end, the equivariance loss can be introduced by measuring the distance between two sides of Equ. (7) as

$$\mathcal{L}_{\text{equi}}^{(G,\Phi)} = \mathbb{E}_{\mathbf{z}, \mathbf{c}, \epsilon} \mathcal{L}_{\text{percep}}(G(\mathcal{T}_\epsilon^Z \mathbf{z}, \mathbf{c}), \mathcal{T}_\epsilon^X G(\mathbf{z}, \mathbf{c})), \quad (8)$$

where $\mathcal{L}_{\text{percep}}(\cdot, \cdot)$ is the perceptual loss defined as $\mathcal{L}_{\text{percep}}(\mathbf{x}, \mathbf{y}) = \sum_{l=0}^L \frac{1}{|\Omega_l|} \sum_{u \in \Omega_l} \left\| \Gamma_u^{(l)}(\mathbf{x}) - \Gamma_u^{(l)}(\mathbf{y}) \right\|_2^2$, where $\Gamma_u^{(l)}(\cdot)$ denotes the normalized feature at index u on the l -th layer feature map of a pre-trained neural network and $\Gamma_u^{(0)}(\cdot)$ represents the input image. We adopt a neural network pre-trained with self-supervised task [17] on ImageNet to avoid introducing external supervision.¹

3.3. Learning

The Equivariant Layered GAN (ELGAN) is trained by alternating the following two steps,

$$\begin{aligned} \min_{G, E, \Phi} \mathcal{L}_{\text{adv}}^{(G)} + \gamma_r \mathcal{L}_r^{(G,E)} + \gamma_b \mathcal{L}_b^{(G)} + \gamma_e(t) \mathcal{L}_{\text{equi}}^{(G,\Phi)} + \gamma_{\text{reg}} \mathcal{L}_{\text{reg}}^{(\Phi)} \\ \min_D \mathcal{L}_{\text{adv}}^{(D)}, \end{aligned} \quad (9)$$

where γ denotes the loss weights and $\mathcal{L}_{\text{adv}}^{(\cdot)}$ is the adversarial loss with perturbation Equ. (3) applied. We use hinge loss, *i.e.* $\mathcal{L}_{\text{adv}}^{(G)} = -\mathbb{E}_{\mathbf{z}} D(\mathcal{T}_\epsilon^X G(\mathbf{z}, \mathbf{c}))$ and $\mathcal{L}_{\text{adv}}^{(D)} = \mathbb{E}_{p_{\text{data}}(\mathbf{x})} \max(0, 1 - D(\mathbf{x})) + \mathbb{E}_{\mathbf{z}} \max(0, 1 + D(\mathcal{T}_\epsilon^X G(\mathbf{z}, \mathbf{c})))$. $\mathcal{L}_r^{(G,E)}$ is defined by Equ. (6), $\mathcal{L}_b^{(G)}$ is the binarisation loss $\mathcal{L}_b^{(G)} = \mathbb{E}_{\mathbf{z}, \mathbf{c}} \min\{\pi, \mathbf{1} - \pi\}$ to encourage the binarization of masks, $\mathcal{L}_{\text{equi}}^{(G,\Phi)}$ is the equivariance loss Equ. (8), and $\mathcal{L}_{\text{reg}}^{(\Phi)}$ is a regularization term which will be explained later.

In practice, it is essential to enforce the equivariance more when the foreground-background separation is more stable. Therefore, we use a linear ramp up schedule for the equivariance loss weight $\gamma_e(t) = \min(1, \frac{t}{t_1}) \gamma_{\text{equi}}$, where

¹We use a RotNet [17] pretrained VGG16 model obtained from <https://github.com/facebookresearch/DeeperCluster>.

t and t_1 denote the current training epoch and the ending epoch of the ramp up schedule. We also observe that without any restriction $\mathcal{T}_\epsilon^{\mathcal{Z}}\mathbf{z}$ often lie out of the distribution of \mathbf{z} with its statistics exploding. Therefore, we introduce an additional loss term to regularize the estimated first and second moments of $\mathcal{T}_\epsilon^{\mathcal{Z}}\mathbf{z}$ over a mini-batch of N samples. Formally, $\mathcal{L}_{\text{reg}}^{(\Phi)} = \left\| \frac{1}{N} \sum_{i=1}^N \mathcal{T}_{\epsilon_i}^{\mathcal{Z}} \mathbf{z}_i \right\|_2^2 + \left\| \frac{1}{N} \sum_{i=1}^N (\mathcal{T}_{\epsilon_i}^{\mathcal{Z}} \mathbf{z}_i)^2 - 1 \right\|_2^2$.

3.4. Unsupervised Foreground-Background Segmentation

After the Equivariant Layered GAN is trained, the pseudo-segmentation dataset $\{(x_i, \pi_i)\}_{i=1}^N$ is synthesized by drawing latent variables $\{z_i\}_{i=1}^N \sim \mathcal{N}(0, 1)$ and $\{c_i\}_{i=1}^N \sim \text{Cat}(d_c, 1/d_c)$ and forwarding $\{(z_i, c_i)\}_{i=1}^N$ to the generator G . A segmentation network $F_\theta : \mathcal{X} \rightarrow [0, 1]^{H \times W}$ parameterized with θ is optimized as follows,

$$\min_{\theta} \frac{1}{N} \sum_{i=1}^N (1 - \pi_i) \log(1 - F_\theta(x_i)) + \pi_i \log(F_\theta(x_i)). \quad (10)$$

Since the layered GAN approximates the real data distribution and produces reasonable masks, the optimized F_θ could fairly generalize to handle real images.

4. Experiments

4.1. Settings

Datasets. Our methods are evaluated on *Caltech-UCSD Birds 200-2011* (CUB) [59] and *LSUN Car* [62], which are one-class datasets where most images contain single object. Though it is far away from real-world application, we have to start with these simple datasets regarding the significant difficulty of unsupervised segmentation. Following Chen *et al.* [7], CUB is split into 10,000 training images, 788 validation images, and 1,000 testing images. Following Savarese *et al.* [49], a subset of 1,040 images in LSUN Car are reserved for test. While ground-truth object masks are available in CUB, ground-truth masks in LSUN Car are approximated by pre-trained Mask R-CNN which are provided by Savarese *et al.* [49]. The segmentation performance on the test set is evaluated and reported, where we follow previous work [7, 49] to resize and center crop the original image to 128×128 resolution.

Implementation details. Our GAN structure is adapted from FineGAN [53]. The dimension of \mathbf{z} is 100 while the dimension of \mathbf{c} is 200. By default, we set $\gamma_r = 1$, $\gamma_b = 2$, $\gamma_{\text{equi}} = 0.5$. For the perturbation, we sample scaling parameter $\log_2 s \sim \mathcal{U}(-0.2, 0.2)$ and translation parameter $t_x, t_y \sim \mathcal{U}(-0.125, 0.125)$. The GAN is trained

Methods	CUB			LSUN Car		
	ACC	IoU	mIoU	ACC	IoU	mIoU
Voynov <i>et al.</i> [58]	94.0	71.0	-	-	-	-
Supervised U-Net	98.0	88.8	93.2	95.1	91.2	90.5
GrabCut [46] by [49]	72.3	36.0	52.3	69.1	57.6	53.4
ReDO [7]	84.5	42.6	-	-	-	-
PerturbGAN [3]	-	-	38.0	-	-	54.0
IEM + SegNet [49]	89.3	55.1	71.4	77.8	68.5	63.2
ELGAN + U-Net (ours)	93.3	67.1	79.7	76.7	66.8	61.5

Table 1: Unsupervised object segmentation performance. “-” suggests that the number is not reported in the original paper.

at 128×128 resolution by Adam [32] optimizer with initial learning rate as 0.0002 and (β_1, β_2) as (0.5, 0.999). The default batch size is set as 32. Following [57], U-Net [45] is used as segmentation network. More details are explained in the supplementary material.

Evaluation metrics. We evaluate the segmentation performance with three metrics, per-pixel mean accuracy (ACC), intersection over union (IoU) between predicted and ground-truth foreground masks, and mean IoU (mIoU) over foreground and background. For image generation performance, FID [21], precision and recall [34] of 10k generated images against a subset of 10k training images are used to indicate the discrepancy between fake and real data distribution, the fidelity of fake images, and the diversity of the fake images respectively. The reported performance is evaluated on the checkpoints with lowest FID during training process. The lowest-FID model is also utilized to synthesize pseudo-segmentation training data.

4.2. Unsupervised Object Segmentation

The segmentation performance is quantitatively measured and compared to prior work in Table 1. The results of Voynov *et al.* [58] and the upper bound, *i.e.* supervised U-Net, are also listed for reference. Voynov *et al.* [58] require manual inspection which implies external supervision, thus not fairly comparable to the others. The results show that our methods outperform our baseline method, PerturbGAN [3], and previous work [7] by a large margin. Compared to the most recent work [49], our performance is significantly stronger on CUB dataset where background is less complicated, yet very close on LSUN Car dataset where more wild images with complicated background exist. The techniques of our methods are orthogonal to [49]. We believe that they could be integrated to push the performance of unsupervised segmentation even higher in the future.

Some qualitative results are presented in Fig.5 and more

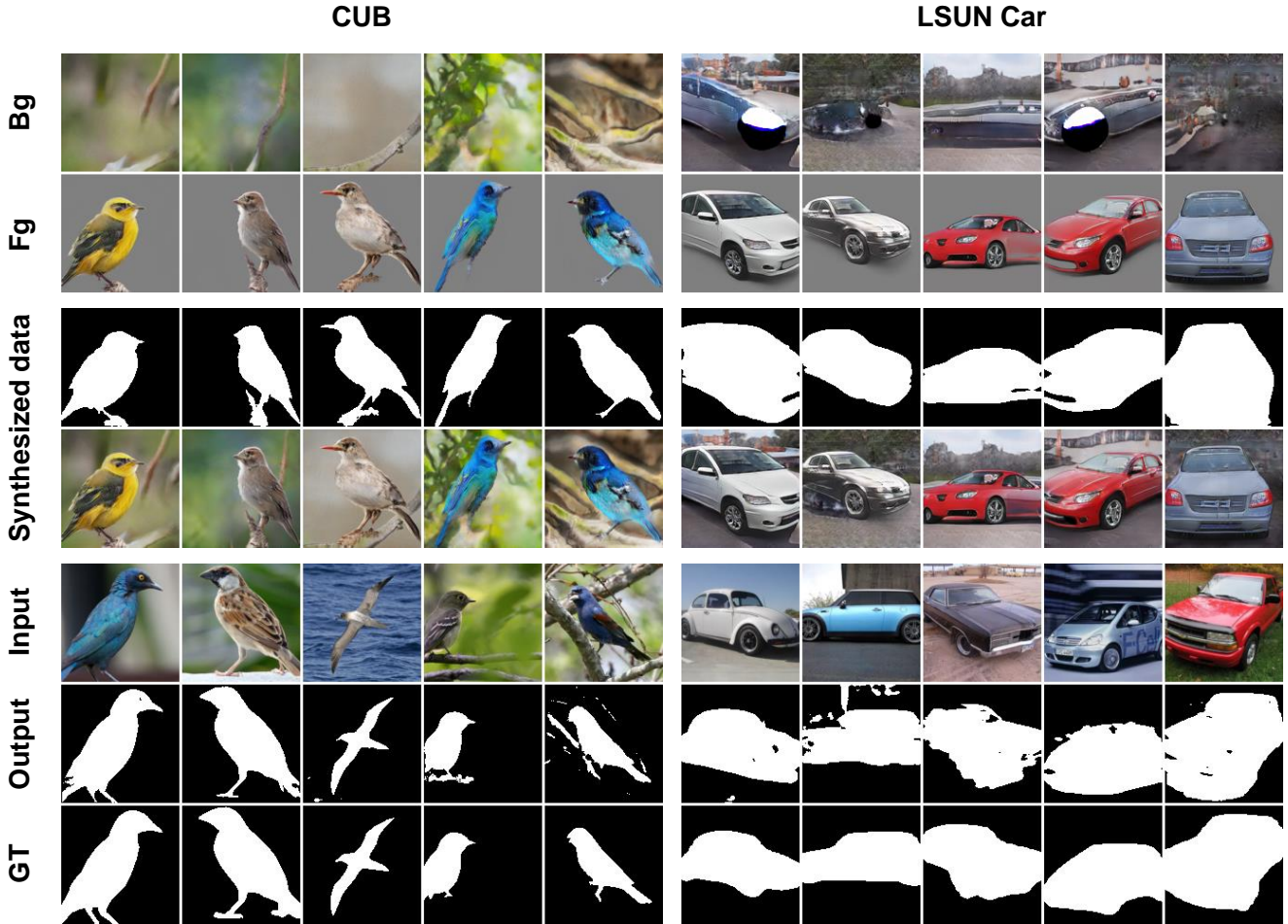


Figure 5: Qualitative results. Examples of generated background (Bg), foreground (Fg), mask and image are presented. The masks and images are used as synthetic data. At the last three rows, the real test images (Input), predicted masks by U-Net (Output), and ground truth masks (GT) are presented.

results are available in the supplementary material. These results show that our Equivariant Layered GANs could generate photo-realistic synthetic images with reasonable foreground masks which leads to a segmentation network able to perform foreground-background segmentation on realistic test images. Our methods produce holistic object masks that can represent the object entities due to their generative nature. The segmentation results on real test images are of high quality but not as perfect as synthesized masks, possibly due to the realness gap between the fake images and real images, which undermines the generalization to real images. We believe with the advance of fundamental GAN techniques, the unsupervised segmentation results could be further improved.

4.3. Image Generation

Qualitative results in Fig. 5 show that our GANs learn to disentangle foreground and background. Quantitative re-

Datasets	FID ↓	Precision ↑	Recall ↑
CUB	15.7	70.3	9.9
LSUN Car	31.9	66.4	4.31

Table 2: Quantitative evaluation of the generation.

sults are also listed in Tab. 2 for reference. Since our GAN takes two latent variables z and c as input, it is explored if the latent variables could be related to certain semantics and results are shown in Fig. 6. Since z is public across background and foreground and c is only private to foreground, varying c does not alter the background while varying z could change the whole background and some details in foreground. Furthermore, it can be observed that images generated from the same c are common in shape, texture, characteristic color, etc, implying that c might represent some potential clustering learned by the model.

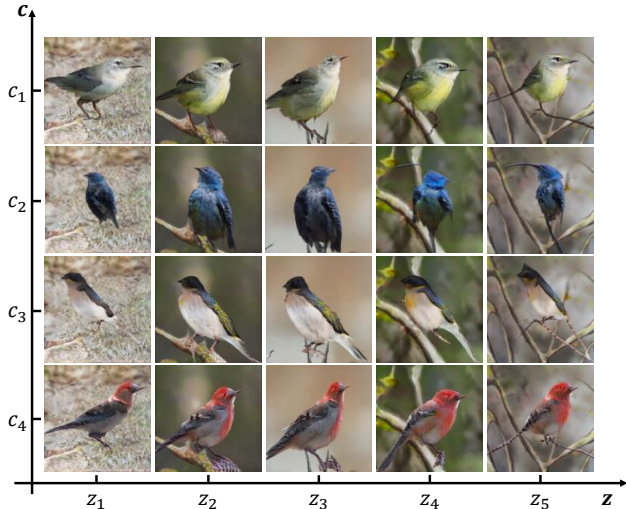


Figure 6: Examples of controlled generation. public code z and private code c are changed separately.



Figure 7: The images are generated by interpolating z in a specific equivariant direction. Training process only covers the transformation range $[-1, +1]$.

Since equivariance loss is enforced, it is also explored if certain directions in z latent space could be interpreted as geometric transformation. A direction in the latent space is acquired by forwarding $\epsilon \in \mathcal{E}$ to Φ . Interpolating along the direction results in the generated images shown in Fig. 7. Note that the latent directions could even be interpreted out of the small range of ϵ (denoted as $[-1, +1]$ in Fig. 7) covered by the training process, despite less accuracy and less disentanglement. Equivariance does not perfectly hold everywhere in the latent space but approximately holds in a small range, which already benefits segmentation a lot. We believe stronger equivariance could bring more improvement, which is left as future work.

4.4. Ablation Study

Ablation study is conducted on CUB dataset at 64×64 resolution and the results are presented in Tab. 3. It begins with a counterpart of PerturbGAN [3], *i.e.* configuration A,

	Configuration	FID ↓	IoU ↑
A	Base (counterpart of [3])	23.2	38.5
B	A $-\mathcal{L}_{\text{size}}^{(G)} + \mathcal{L}_r^{(G,E)}$	20.9	45.8
C	B + $\mathcal{S}(s)$	18.2	57.3
D	C + $\mathcal{R}(\alpha)$	18.4	58.1
E	C + $\mathcal{L}_e^{(G,\Phi)}$ (ELGAN)	15.4	66.0

Table 3: Ablation study. Starting from A, a counterpart of PerturbGAN [3], we sequentially (B) replace mask size loss with private code recovery, (C) add scale, (D) add rotation, and (E) add equivariance loss.

which adopts mask size loss and translation perturbation as measure to prevent degeneration while has different network structure, mask inference method, and implementation details. Based on A, the mask size loss $\mathcal{L}_{\text{size}}^{(G)}$ is replaced with private code recovery module (denoted as $-\mathcal{L}_{\text{size}}^{(G)} + \mathcal{L}_r^{(G,E)}$), which leads to configuration B. The significant improvement from A to B suggests that the our private code recovery is a more powerful alternative to $\mathcal{L}_{\text{size}}^{(G)}$. Based on B, the scale and rotation are incrementally added (denoted as $+\mathcal{S}(s)$ & $+\mathcal{R}(\alpha)$), which leads to configuration C & D. The increased performance suggests that richer perturbation is helpful for disentangling foreground and background. Note that the improvement from C to D becomes marginal, indicating the benefits of perturbation start to saturate. Finally, we add equivariance loss (denoted) based on D, leading to configuration E. The improvement of segmentation performance from D to E suggests that our proposed equivariance loss helps to a better separation of foreground and background.

5. Conclusion

In this paper, we tackle the unsupervised foreground-background segmentation by training segmentation networks on fake dataset synthesized by Equivariant Layered GAN (ELGAN). ELGAN is based on PerturbGAN with following two main improvements. First, the layer perturbation is extended to a richer set of transformation and a novel private code recovery module is employed to prevent the training from degeneration. Second, an equivariance loss is introduced to make the latent space interpretable and disentangled, which is shown to also benefit the separation of foreground and background. Experiment results show that our method could reasonably perform segmentation on one-class dataset and is competitive compared to state-of-the-art methods. Our method can potentially be used in multi-category and multi-instance cases after integrated into weakly supervised object detection methods, which is left as future work.

References

- [1] Bogdan Alexe, Thomas Deselaers, and Vittorio Ferrari. Classcut for unsupervised class segmentation. In *ECCV*, 2010. 1, 2
- [2] Yaniv Benny and Lior Wolf. Onegan: Simultaneous unsupervised learning of conditional image generation, foreground segmentation, and fine-grained clustering. In *ECCV*, 2020. 3
- [3] Adam Bielski and Paolo Favaro. Emergence of object segmentation in perturbed generative models. In *NeurIPS*, 2019. 1, 2, 3, 4, 5, 6, 8
- [4] Joan Bruna and Stéphane Mallat. Invariant scattering convolution networks. *TPAMI*, 2013. 3
- [5] Christopher P Burgess, Loic Matthey, Nicholas Watters, Rishabh Kabra, Irina Higgins, Matt Botvinick, and Alexander Lerchner. Monet: Unsupervised scene decomposition and representation. *arXiv preprint arXiv:1901.11390*, 2019. 2
- [6] Yuning Chai, Victor Lempitsky, and Andrew Zisserman. Bicos: A bi-level co-segmentation method for image classification. In *ICCV*, 2011. 1, 2
- [7] Mickaël Chen, Thierry Artières, and Ludovic Denoyer. Unsupervised object segmentation by redrawing. In *NeurIPS*, 2019. 1, 2, 6, 11, 12
- [8] Xi Chen, Yan Duan, Rein Houthoofd, John Schulman, Ilya Sutskever, and Pieter Abbeel. Infogan: Interpretable representation learning by information maximizing generative adversarial nets. In *NIPS*, 2016. 5, 11
- [9] Zezhou Cheng, Jong-Chyi Su, and Subhransu Maji. Unsupervised discovery of object landmarks via contrastive learning. *arXiv preprint arXiv:2006.14787*, 2020. 3
- [10] Benjamin Chidester, That-Vinh Ton, Minh-Triet Tran, Jian Ma, and Minh N Do. Enhanced rotation-equivariant u-net for nuclear segmentation. In *CVPR Workshops*, 2019. 3
- [11] Taco Cohen, Mario Geiger, and Maurice Weiler. A general theory of equivariant cnns on homogeneous spaces. In *NIPS*, 2019. 3
- [12] Taco Cohen and Max Welling. Group equivariant convolutional networks. In *ICML*, 2016. 3
- [13] Neel Dey, Antong Chen, and Soheil Ghafurian. Group equivariant generative adversarial networks. In *ICLR*, 2021. 3
- [14] Jeff Donahue and Karen Simonyan. Large scale adversarial representation learning. In *Advances in Neural Information Processing Systems*, pages 10542–10552, 2019. 2
- [15] Martin Engelcke, Adam R Kosiorek, Oiwi Parker Jones, and Ingmar Posner. Genesis: Generative scene inference and sampling with object-centric latent representations. In *ICLR*, 2020. 2
- [16] S. M. Ali Eslami, Nicolas Heess, Theophane Weber, Yuval Tassa, David Szepesvari, koray kavukcuoglu, and Geoffrey E Hinton. Attend, infer, repeat: Fast scene understanding with generative models. In *NIPS*. 2016. 3
- [17] Spyros Gidaris, Praveer Singh, and Nikos Komodakis. Unsupervised representation learning by predicting image rotations. In *International Conference on Learning Representations*, 2018. 3, 5
- [18] Lore Goetschalckx, Alex Andonian, Aude Oliva, and Phillip Isola. Analyze: Toward visual definitions of cognitive image properties. In *Proceedings of the IEEE International Conference on Computer Vision*, pages 5744–5753, 2019. 3
- [19] Ian Goodfellow, Jean Pouget-Abadie, Mehdi Mirza, Bing Xu, David Warde-Farley, Sherjil Ozair, Aaron Courville, and Yoshua Bengio. Generative adversarial nets. In *Advances in neural information processing systems*, pages 2672–2680, 2014. 1, 2
- [20] Klaus Greff, Raphaël Lopez Kaufmann, Rishabh Kabra, Nick Watters, Christopher Burgess, Daniel Zoran, Loic Matthey, Matthew Botvinick, and Alexander Lerchner. Multi-object representation learning with iterative variational inference. In *ICML*, 2019. 2
- [21] Martin Heusel, Hubert Ramsauer, Thomas Unterthiner, Bernhard Nessler, and Sepp Hochreiter. Gans trained by a two time-scale update rule converge to a local nash equilibrium. In *NeurIPS*, 2017. 6
- [22] Geoffrey E Hinton, Sara Sabour, and Nicholas Frosst. Matrix capsules with em routing. In *ICLR*, 2018. 3
- [23] Dorit S Hochbaum and Vikas Singh. An efficient algorithm for co-segmentation. In *ICCV*, 2009. 1, 2
- [24] Wei-Chih Hung, Varun Jampani, Sifei Liu, Pavlo Molchanov, Ming-Hsuan Yang, and Jan Kautz. Scops: Self-supervised co-part segmentation. In *CVPR*, 2019. 3
- [25] Erik Härkönen, Aaron Hertzmann, Jaakko Lehtinen, and Sylvain Paris. Ganspace: Discovering interpretable gan controls. In *Proc. NeurIPS*, 2020. 3, 5
- [26] Ali Jahanian, Lucy Chai, and Phillip Isola. On the “steerability” of generative adversarial networks. In *ICLR*, 2020. 3, 5
- [27] Xu Ji, João F Henriques, and Andrea Vedaldi. Invariant information clustering for unsupervised image classification and segmentation. In *ICCV*, 2019. 1, 2
- [28] Armand Joulin, Francis Bach, and Jean Ponce. Discriminative clustering for image co-segmentation. In *CVPR*, 2010. 1, 2
- [29] Tero Karras, Samuli Laine, and Timo Aila. A style-based generator architecture for generative adversarial networks. In *Proceedings of the IEEE conference on computer vision and pattern recognition*, pages 4401–4410, 2019. 3
- [30] Tero Karras, Samuli Laine, Miika Aittala, Janne Hellsten, Jaakko Lehtinen, and Timo Aila. Analyzing and improving the image quality of stylegan. In *CVPR*, 2020. 11
- [31] Wonjik Kim, Asako Kanezaki, and Masayuki Tanaka. Unsupervised learning of image segmentation based on differentiable feature clustering. *TIP*, 2020. 1, 2
- [32] Diederik P Kingma and Jimmy Ba. Adam: A method for stochastic optimization. *arXiv preprint arXiv:1412.6980*, 2014. 6, 12
- [33] Diederik P Kingma and Max Welling. Auto-encoding variational bayes. In *ICLR*, 2014. 2
- [34] Tuomas Kynkäänniemi, Tero Karras, Samuli Laine, Jaakko Lehtinen, and Timo Aila. Improved precision and recall metric for assessing generative models. In *NeurIPS*, 2019. 6
- [35] Karel Lenc and Andrea Vedaldi. Understanding image representations by measuring their equivariance and equivalence.

- In *Proceedings of the IEEE conference on computer vision and pattern recognition*, pages 991–999, 2015. 2, 3, 5
- [36] Zinan Lin, Kiran Thekumparampil, Giulia Fanti, and Se-woong Oh. Infogan-cr and modelcentrality: Self-supervised model training and selection for disentangling gans. In *ICML*, 2020. 5, 11
- [37] Zhixuan Lin, Yi-Fu Wu, Skand Vishwanath Peri, Weihao Sun, Gautam Singh, Fei Deng, Jindong Jiang, and Sungjin Ahn. Space: Unsupervised object-oriented scene representation via spatial attention and decomposition. 2020. 2
- [38] Jasper Linmans, Jim Winkens, Bastiaan S Veeling, Taco S Cohen, and Max Welling. Sample efficient semantic segmentation using rotation equivariant convolutional networks. *arXiv preprint arXiv:1807.00583*, 2018. 3
- [39] Octave Mariotti and Hakan Bilen. Semi-supervised viewpoint estimation with geometry-aware conditional generation. In *ECCV Workshop*, 2020. 2
- [40] Takeru Miyato, Toshiki Kataoka, Masanori Koyama, and Yuichi Yoshida. Spectral normalization for generative adversarial networks. In *ICLR*, 2018. 11
- [41] Yassine Ouali, Céline Hudelot, and Myriam Tami. Autoregressive unsupervised image segmentation. In *ECCV*, 2020. 1, 2
- [42] Edouard Oyallon and Stéphane Mallat. Deep roto-translation scattering for object classification. In *CVPR*, 2015. 3
- [43] Antoine Plumerault, Hervé Le Borgne, and Céline Hudelot. Controlling generative models with continuous factors of variations. In *ICLR*, 2020. 3
- [44] Alec Radford, Luke Metz, and Soumith Chintala. Unsupervised representation learning with deep convolutional generative adversarial networks. *arXiv preprint arXiv:1511.06434*, 2015. 3
- [45] Olaf Ronneberger, Philipp Fischer, and Thomas Brox. U-net: Convolutional networks for biomedical image segmentation. In *MICCAI*, 2015. 6, 12
- [46] Carsten Rother, Vladimir Kolmogorov, and Andrew Blake. ” grabcut” interactive foreground extraction using iterated graph cuts. *TOG*, 2004. 6
- [47] Carsten Rother, Tom Minka, Andrew Blake, and Vladimir Kolmogorov. Cosegmentation of image pairs by histogram matching-incorporating a global constraint into mrfs. In *CVPR*, 2006. 1, 2
- [48] Sara Sabour, Nicholas Frosst, and Geoffrey E Hinton. Dynamic routing between capsules. In *NIPS*, 2017. 3
- [49] Pedro Savarese, Sunnie SY Kim, Michael Maire, Greg Shakhnarovich, and David McAllester. Information-theoretic segmentation by inpainting error maximization. *arXiv preprint arXiv:2012.07287*, 2020. 2, 6, 12
- [50] Andrew M Saxe, James L McClelland, and Surya Ganguli. Exact solutions to the nonlinear dynamics of learning in deep linear neural networks. *arXiv preprint arXiv:1312.6120*, 2013. 11
- [51] Yujun Shen, Jinjin Gu, Xiaou Tang, and Bolei Zhou. Interpreting the latent space of gans for semantic face editing. In *Proceedings of the IEEE/CVF Conference on Computer Vision and Pattern Recognition*, pages 9243–9252, 2020. 3, 5
- [52] Laurent Sifre and Stéphane Mallat. Rotation, scaling and deformation invariant scattering for texture discrimination. In *CVPR*, 2013. 3
- [53] Krishna Kumar Singh, Utkarsh Ojha, and Yong Jae Lee. Finegan: Unsupervised hierarchical disentanglement for fine-grained object generation and discovery. In *Proceedings of the IEEE Conference on Computer Vision and Pattern Recognition*, pages 6490–6499, 2019. 3, 6, 11
- [54] Nurit Spingarn-Eliezer, Ron Banner, and Tomer Michaeli. Gan steerability without optimization. *ICLR*, 2021. 3
- [55] James Thewlis, Hakan Bilen, and Andrea Vedaldi. Unsupervised learning of object frames by dense equivariant image labelling. In *Advances in neural information processing systems*, pages 844–855, 2017. 2, 3
- [56] Bastiaan S Veeling, Jasper Linmans, Jim Winkens, Taco Cohen, and Max Welling. Rotation equivariant cnns for digital pathology. In *MICCAI*, 2018. 3
- [57] Andrey Voynov and Artem Babenko. Unsupervised discovery of interpretable directions in the gan latent space. In *ICML*, 2020. 3, 5, 6
- [58] Andrey Voynov, Stanislav Morozov, and Artem Babenko. Big gans are watching you: Towards unsupervised object segmentation with off-the-shelf generative models. *arXiv preprint arXiv:2006.04988*, 2020. 1, 2, 3, 6, 12
- [59] C. Wah, S. Branson, P. Welinder, P. Perona, and S. Belongie. The Caltech-UCSD Birds-200-2011 Dataset. Technical Report CNS-TR-2011-001, California Institute of Technology, 2011. 6
- [60] Daniel E Worrall, Stephan J Garbin, Daniyar Turmukhambetov, and Gabriel J Brostow. Interpretable transformations with encoder-decoder networks. In *ICCV*, 2017. 2
- [61] Jianwei Yang, Anitha Kannan, Dhruv Batra, and Devi Parikh. Lr-gan: Layered recursive generative adversarial networks for image generation. *arXiv preprint arXiv:1703.01560*, 2017. 3
- [62] Fisher Yu, Ari Seff, Yinda Zhang, Shuran Song, Thomas Funkhouser, and Jianxiong Xiao. Lsun: Construction of a large-scale image dataset using deep learning with humans in the loop. *arXiv preprint arXiv:1506.03365*, 2015. 6
- [63] Liheng Zhang, Guo-Jun Qi, Liqiang Wang, and Jiebo Luo. Aet vs. aed: Unsupervised representation learning by auto-encoding transformations rather than data. In *Proceedings of the IEEE Conference on Computer Vision and Pattern Recognition*, pages 2547–2555, 2019. 3
- [64] Shengyu Zhao, Zhijian Liu, Ji Lin, Jun-Yan Zhu, and Song Han. Differentiable augmentation for data-efficient gan training. In *NeurIPS*, 2020. 12

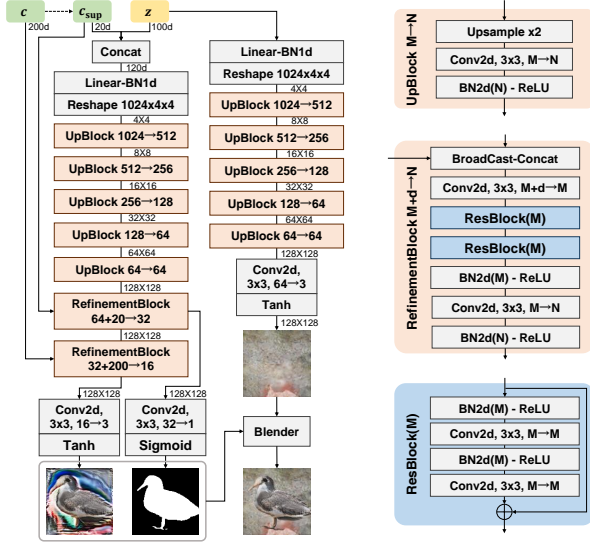


Figure A.1: Structure of our generator.

A. Implementation Details

Generator. The structure of our generator (Fig. A.1) is adapted from FineGAN [53] which is tailored for generating images of fine-grained categories. Compared to the original structure, the GRU activation function is replaced with ReLU to save some computation without sacrificing too much performance. In this structure, the pseudo category c is grouped into super categories c_{sup} with group size 10, which means 10 consecutive c 's would be grouped into one super category. Apart from z , only c_{sup} has impacts on the generated masks, whereas c_{sup} and c have impacts on the foreground appearance, *i.e.* RGB value. The weights of all the convolutional and linear layers are initialized with orthogonal matrix [50].

Discriminator and private code recovery. The structures of our discriminator and private code recovery are presented in Fig. A.2. The basic private code c is recovered from the generated image as \hat{c} while the super category c_{sup} is recovered from the generated mask as \hat{c}_{sup} . Following InfoGAN [8] and its variant [36], the c recovery module shares the backbone network with the discriminator. The c_{sup} recovery module is constructed with an independent neural network with takes as input the generated masks and output the reconstructed super category \hat{c}_{sup} . To stabilize the training, spectral normalization [40] is applied to all the layers in discriminator and private coder recovery modules. The weights of all the convolutional and linear layers are initialized with orthogonal matrix [50].

Latent transformation model. During training process, the transformation index $\epsilon \in [-1, 1]^{d_\epsilon}$ is drawn from a uni-

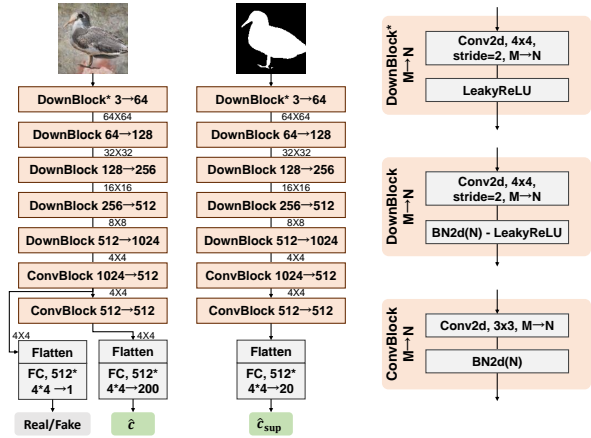


Figure A.2: Structure of our discriminator and private code recovery. Discriminator and c recovery module share the first six blocks. Another c_{sup} recovery module is introduced, which take as input the generated masks and reconstruct the source super category as \hat{c}_{sup} .

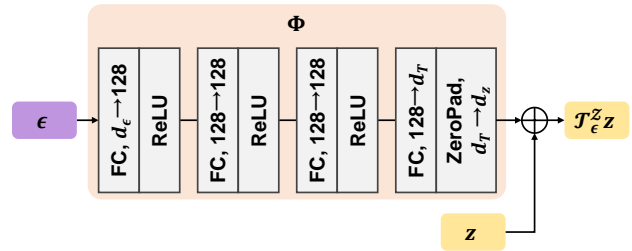


Figure A.3: Structure of our latent transformation model. d_ϵ , d_T , and d_z represent the dimensions of ϵ , transformation, and z respectively.

form distribution as $\epsilon \sim \mathcal{U}[-1, 1]^{d_\epsilon}$, where the dimension d_ϵ conforms to the degrees of affine transformation. For example, if only translation is enabled, then $d_\epsilon = 2$; if translation, scaling and rotation are enabled, then $d_\epsilon = 4$. The latent transformation \mathcal{T}_ϵ^z is modeled as $\mathcal{T}_\epsilon^z z = z + \Phi(\epsilon)$, where Φ is implemented with a 4-layer Multiple Layer Perceptron (MLP) as in Fig. A.3. It is found that restricting the transformation to a subspace of \mathcal{Z} helps to stabilize training. Therefore, \mathcal{T}_ϵ^z is restricted to only changing the first 10 dimensions of z , *i.e.* $d_T = 10$ in Fig. A.3.

Dataset and augmentation. Following the dataset split provided by Chen *et al.* [7], 10,000 images are used for training. In LSUN Car, following [30], images of size around 533×400 in the first 200k images are used as training images, which result in 31,893 training images. The number of training images is further doubled by horizontally flipping every image, and augmented

by `RandomResizedCrop`². This augmentation could slightly increase the variation in the training images and is helpful considering that the layer perturbation is used during training. Moreover, the color augmentation technique proposed by Zhao *et al.* [64] for training GAN is also applied.

Optimization of GAN. Since the super private code \mathbf{c}_{sup} is introduced, the recovery loss $\mathcal{L}_r^{(G,E)}$ is extended to two terms which represent \mathbf{c} recovery and \mathbf{c}_{sup} recovery respectively, and E collectively represents the \mathbf{c} recovery module E_x and \mathbf{c}_{sup} recovery module E_π , *i.e.* $E = (E_x, E_\pi)$. Formally,

$$\mathcal{L}_r^{(G,E)} = \mathbb{E}_{\mathbf{z}, \mathbf{c}} \left[-\log E_x(\mathbf{c}|G(\mathbf{z}, \mathbf{c})) - \log E_\pi(\mathbf{c}_{\text{sup}}|G_f^{(\pi)}(\mathbf{z}, \mathbf{c})) \right]. \quad (11)$$

The loss weights are set as $\gamma_r = 1$, $\gamma_b = 2$, $\gamma_{\text{equi}} = 0.5$ for both datasets. The perturbation parameters are sampled as $\log_2 s \sim \mathcal{U}(-0.2, 0.2)$ and $t_x, t_y \sim \mathcal{U}(-0.125, 0.125)$. The loss is optimized over mini-batches of 32 real images via stochastic gradient descent by Adam [32] optimizer with initial learning rate as 0.0002 and (β_1, β_2) as (0.5, 0.999). Both the generator and the discriminator operate at 128×128 resolution. The model is trained for 810 epochs on CUB and 81 epochs on LSUN Car. The ending epoch of ramp up schedule of $\gamma_\epsilon(t)$, t_1 , is set as 400 epoch on CUB and 40 epoch on LSUN Car.

Training segmentation network. A simple U-Net architecture [45] is used as segmentation network. Exactly the same as [58], the U-Net is trained on the synthetic dataset by Adam optimizer with initial learning rate as 0.001 and batch size as 95 for 12,000 steps. The learning rate is decreased by 0.2 at the 8,000th step. During inference, following [7, 49], the input image and ground truth masks are rescaled and center cropped to 128×128 .

B. Qualitative Results

Real images. Fig. B.4 presents some examples of training images in CUB and LSUN Car. It can be observed that CUB is a more constrained dataset than LSUN Car in terms of camera views, the wholeness of foreground object, and size of foreground object, the number of foreground objects, and so on. In particular, in LSUN Car, there are a lot of images of truncated cars, multiple cars, and cars occluded by person. Unlike CUB where background is occasionally monochromatic, usually textural, and rarely structural, the LSUN Car dataset contains more complicated and structural background where there could be buildings, streets,

and even other cars. These make the LSUN Car more challenging dataset. According to the results presented in the main text, our methods could also work in the more complicated scenarios and achieve close performance to the state-of-the-art method; they become very strong and surpass state-of-the-art method by a large margin when the dataset is more regular.

Synthesized layers and images. Uncurated examples of generated layers are provided in Fig. B.5 and Fig. B.6. It can be observed that there exists ambiguity about the definition of foreground. Particularly, in CUB, the reflection in the water and tree branches are sometimes taken as foreground and so is the shadow of car in LSUN Car. We think solving such ambiguity issues requires injecting prior knowledge or leveraging extra supervision.

Segmentation results. Uncurated results of segmentation are presented in Fig. B.7 and Fig. B.8. Our methods perform well on CUB but less satisfying on LSUN Car. It can be attributed to that LSUN Car is a more challenging dataset as explained above. Typically, the predicted masks of test image are often fragmentary though the masks in synthetic data are intact, which is more obvious in LSUN Car. We think that this issue arises because there is non-negligible divergence between synthetic data distribution and real data distribution, which impedes the segmentation network from fairly generalizing to test images. With the improvement of GAN structures and other techniques, this issue is promising to be solved.

²A built-in module with the same name could be found in PyTorch library.

CUB

LSUN Car

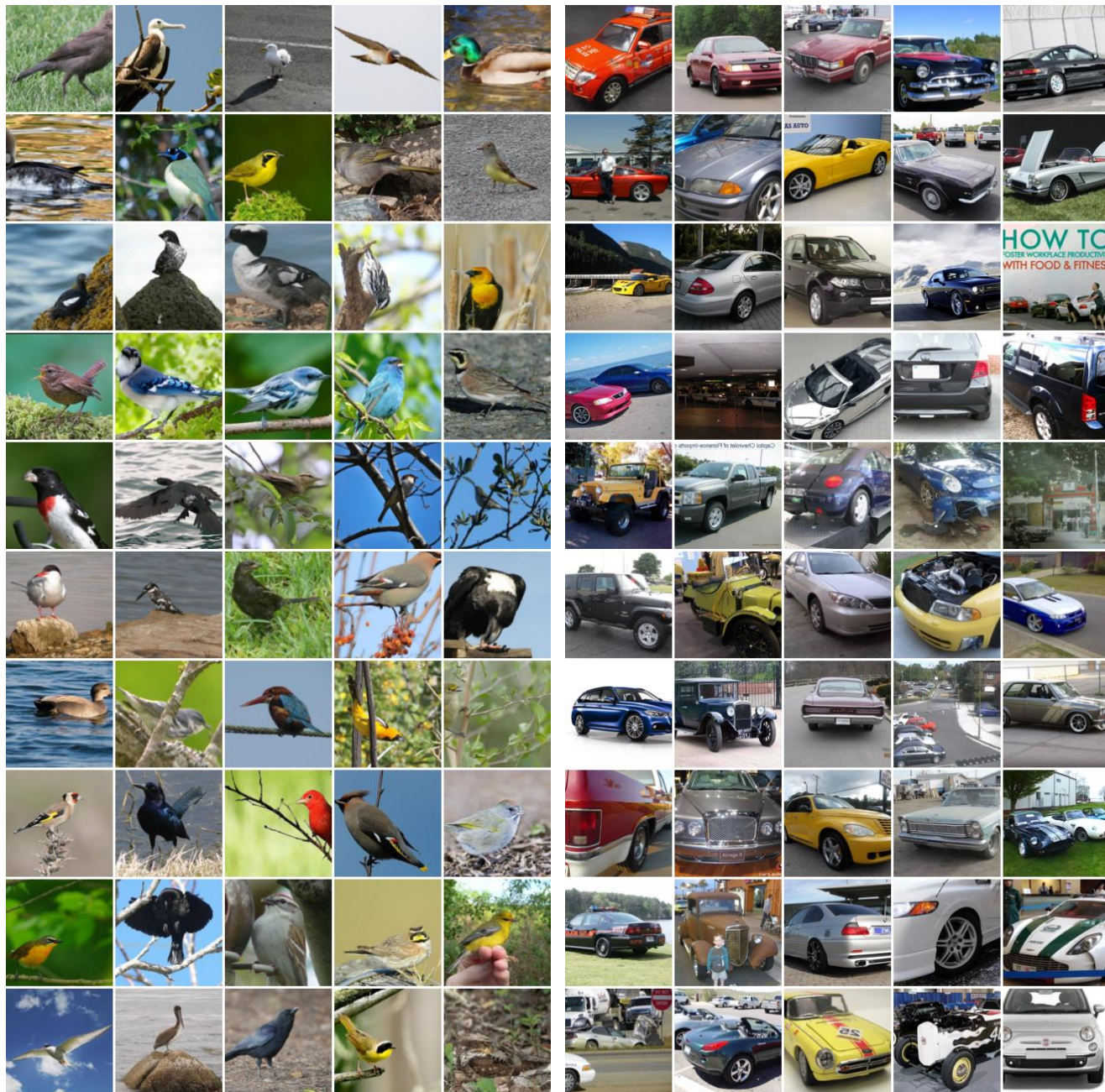


Figure B.4: Uncurated examples of the training images with augmentation randomly applied.

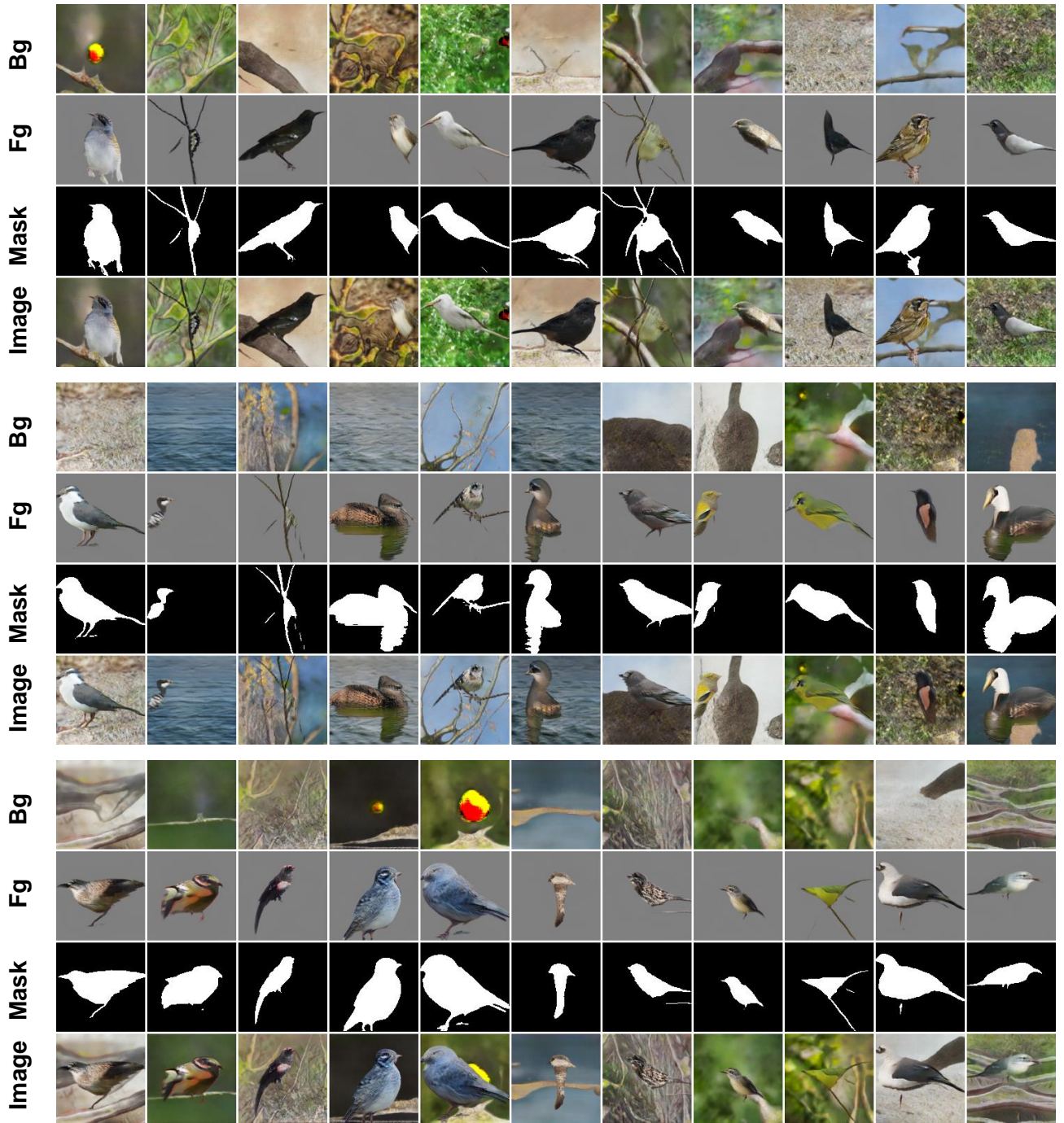


Figure B.5: Uncurated examples of the generated layers (CUB).

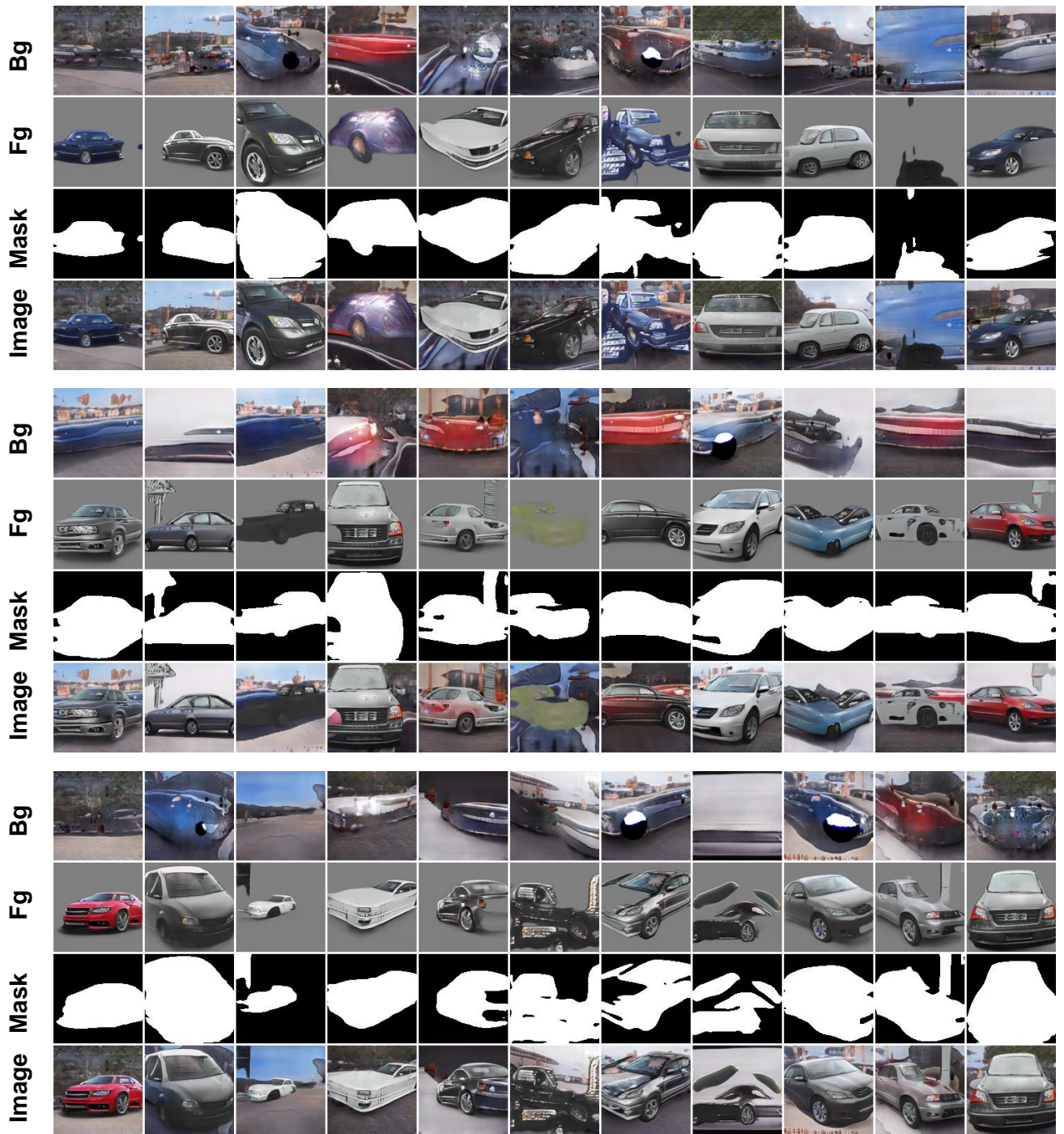


Figure B.6: Uncurated examples of the generated layers (LSUN Car).

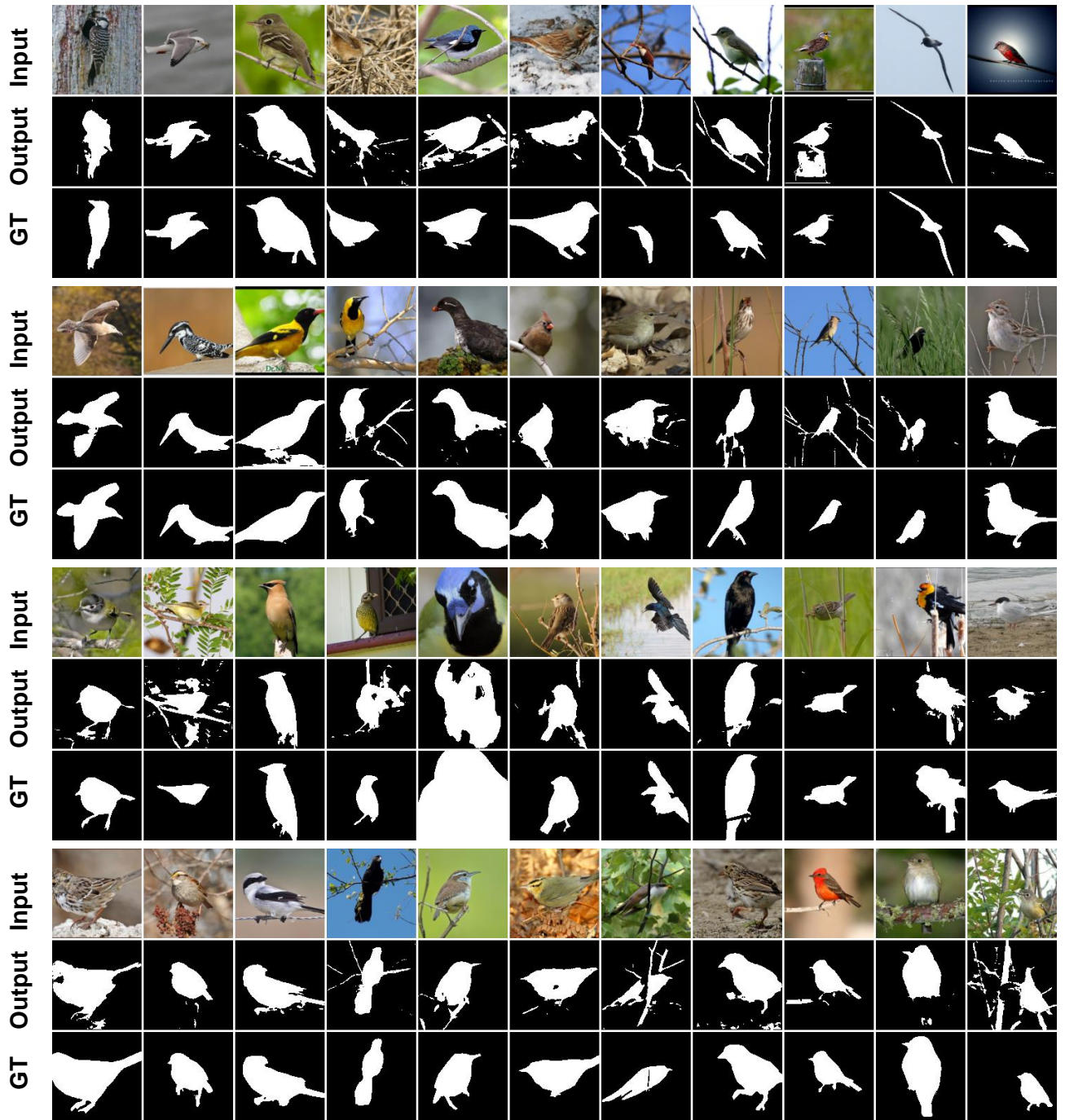


Figure B.7: Uncurated examples of the segmentation on CUB.



Figure B.8: Uncurated examples of the segmentation on LSUN Car.